S & M 4193

Geometric-overlap Modeling and Sweep Uniformity Optimization of Fixed Diamond Conditioning Disks for Chemical Mechanical Planarization

Yu-Chen Wang, Hong-Hui Lian, Yue-Feng Lin, and Ming-Yi Tsai*

Department of Mechanical Engineering, National Chin-Yi University, Zhongshan Rd., Taiping Dist., Taichung 41170, Taiwan

(Received July 14, 2025; accepted October 9, 2025)

Keywords: CMP, diamond conditioning disk, polishing pad dressing uniformity, geometric-overlap model

In this study, we develop a graphics processing unit (GPU)-accelerated geometric-overlap model for fixed-abrasive diamond conditioning disks used in chemical mechanical planarization (CMP). The framework systematically evaluates how diamond-layout strategies and arm-sweep kinematics affect polishing pad coverage uniformity and overall economic performance. A planar rigid-body motion model is first established for diamond chips under the coupled action of disk self-rotation and arm oscillation, and a unified metric, the normalized overlap area ratio (NAR), is defined to quantify radial-sweep uniformity. Simulation conditions are assumed to be a pad diameter of 510 mm, an arm amplitude of ±34°, and a disk speed of 87 rpm; diamond counts from three to twelve are assessed. Trajectory superposition and hit-density statistics are accelerated on a GPU using CuPy. Results show that a single diamond traces an Archimedeanlike spiral, mitigating local wear gradients and impact concentration. With seven to eight diamonds, phase-complementary effects fill the central sweep dead zone, raising NAR to $\approx 30\%$ and optimizing radial and angular uniformities. Integrated cost-performance analysis indicates that a seven- or eight-diamond configuration provides the best trade-off between coverage efficiency and diamond usage; counts above eight lead to excessive overlap in the central region and uneven inner-outer distributions, shortening pad life and raising manufacturing costs, thus driving the system into diminishing returns. The proposed model supplies quantitative guidelines for CMP dresser design, delivering practical benefits for process stability and cost efficiency. These are critical for manufacturing high-performance sensors and devices on advanced material substrates.

1. Introduction

As logic and power devices race from the 10 nm node toward 2 nm and beyond, (1-4) any nanometer-scale deviation in surface profile or film thickness can be magnified during subsequent lithography, etching, and packaging steps, directly degrading electrical uniformity

*Corresponding author: e-mail: mytsai@ncut.edu.tw https://doi.org/10.18494/SAM5844

and product yield. Therefore, chemical mechanical planarization (CMP) has become a decisive step in the sub-10 nm process chain for suppressing error accumulation and maintaining interlayer alignment.^(5,6)

In a CMP system, a diamond conditioning disk periodically conditions the polishing pad to keep the abrasive surface fresh and the removal rate stable.^(7,8) However, conventional electro- or sinter-plated dressers, which are prone to pulling out during long runs, rely on mechanically bonded diamond grit.⁽⁹⁾ Detached diamonds scratch wafer surfaces, become embedded in the pad, and shed metal fragments, raising defect densities, causing cross-metal contamination, and forcing costly tool downtime for cleaning and pad replacement. Worse still, an imbalanced grit density causes removal-rate drift, narrows the process window, and elevates consumable cost,⁽¹⁰⁾ making the dresser a bottleneck for advanced CMP scaling.

Fixed-abrasive diamond conditioning disks have emerged as a remedy.⁽¹¹⁾ Fabricated from CVD single-crystal diamond, micromachined cutting structures are integrated directly into the diamond wafer and brazed into a metal holder, eliminating pull-out and delivering high, stable cutting forces. Field data show lifetimes one to two orders of magnitude longer than those of plated disks, significantly damping process variation. Yet, without the scientific optimization of the microstructure count, orientation phase, and sweep trajectory, fixed abrasive dressers can still leave unconditioned "dead zones" or cause local over-wear, while excessive diamond use inflates cost. Although existing kinematic and wear models offer deep physical insights, they are often computationally intensive, creating a bottleneck in the rapid design-iteration cycle required by industry.^(12–15) Consequently, industry still lacks a fast, quantitative methodology for predicting how dresser geometry and motion affect sweep coverage and radial uniformity from a system-level perspective.

This work fills that gap by developing a graphics processing unit (GPU)-accelerated geometric overlap model. Our approach enables an efficient evaluation of the spatial and temporal distributions of contact points, allowing for a systematic quantification of sweep uniformity for fixed-abrasive diamond conditioning disks. Integrating this model with a cost-aware optimization metric provides an efficient, repeatable, and economically friendly design guide for next-generation nanometer-scale CMP processes, particularly for materials used in advanced sensors and power devices.

2. Theoretical Background and Modeling

2.1 Geometric overlap model between diamond abrasives and polishing pad

At the geometric level, the sweeping motion of diamond abrasives relative to the polishing pad can be treated as a composite planar rigid-body rotation. A fixed reference frame Σ_0 is attached to the pad centroid O; the pad rotates counterclockwise with a constant angular velocity ω_{pad} . The rotation matrix describes its instantaneous attitude.

$$R_{Pad}(t) = R(\theta_{pad}(t)), \ \theta_{pad}(t) = -\omega_{pad}t$$
 (1)

Inside the dresser-arm assembly, the lapping-plate center C_2 revolves around the reference circle center C_1 with the arm angle $\theta_{arm}(t)$, while the plate itself spins about C_2 at the angular velocity ω_{DD} . The definition is given in

$$R_{arm}(t) = R(\theta_{arm}(t)), R_{DD}(t) = R(\theta_{DD}(t)), \theta_{DD}(t) = -\omega_{DD}t,$$
(2)

and let C_2^0 denote the plate center position in Σ_0 when $\theta_{arm}=0$.

The k-th diamond (out of N_d diamonds) has a fixed location in the local plate frame Σ_{DD} .

$$p_k^{loc} = \left(r_{array}\cos\varphi_k, r_{array}\sin\varphi_k\right), \ \varphi_k = \frac{2\pi k}{N_d}$$
 (3)

Applying the successive transformations "plate spin \rightarrow arm revolution \rightarrow pad spin" yields its absolute position in Σ_0 .

$$p_k(t) = R_{Pad}(t)R_{arm}(t) \left\lceil R_{DD}(t)p_k^{loc} + C_2^0 \right\rceil$$
(4)

Because wear analysis concerns the contact geometry relative to the pad, Eq. (4) is transformed back to the pad-fixed frame Σ_{pad} by left-multiplying $R_{pad}^{-1}(t) = R_{pad}^{\top}(t)$:

$$\tilde{p}_k(t) = R_{arm}(t) \left[R_{DD}(t) p_k^{loc} + C_2^0 \right], \tag{5}$$

where $\tilde{p}_k(t) = (\tilde{x}_k(t), \tilde{y}_k(t))^{\top}$ excludes the pad's rigid rotation and thus represents the accurate sweep trajectory of the diamond over the pad. Treating a diamond as a point contact, the number of impacts delivered by the k-th diamond to a surface point (x, y) within the time interval $[t_0, t_f]$ is

$$\rho_{k}(x,y) = \int_{t}^{t_{f}} \delta(x - \tilde{x}_{k}(t)) \delta(y - \tilde{y}_{k}(t)) dt.$$
(6)

The total impact-density function is $\rho_k(x,y) = \sum_{k=0}^{N_d-1} \rho_k(x,y)$. Because Eq. (4) has no closed-form solution, time is discretized at t_n and the impacts are binned into the histogram cell center at (x_i, y_j) , giving the two-dimensional histogram used later to compute the overlap rate and normalized area ratio.

$$H_{ij} = \sum_{k=0}^{N_d-1} \sum_{n} 1 \left(\left| \tilde{x}_k \left(t_n \right) - x_i \right| < \frac{\Delta_x}{2}, \left| \tilde{y}_k \left(t_n \right) - y_j \right| < \frac{\Delta_y}{2} \right)$$
 (7)

2.2 Definitions of overlap rate and normalized area ratio

In the numerical model used in this study, the instantaneous impact positions of all diamond abrasives on the polishing pad recorded in the pad-fixed coordinate frame throughout the simulation were accumulated on a GPU with CuPy into a 300×300 two-dimensional histogram $H(x_i, y_j)$. Because the impact counts span several orders of magnitude, the histogram is visualized with the logarithmic color scale $\log_{10} \left(H(x_i, y_j) + 1 \right)$, thereby retaining spatial information in both high- and low-frequency regions. To evaluate wear uniformity along the radial direction, the program extracts the cross section at y = 0, yielding the data row $\tilde{H}(x_i) = H(x_i, y = 0)$. This row is then amplitude-normalized by its peak value to obtain the overlap rate distribution.

$$O(x_i) = \frac{\tilde{H}(x_i)}{\max_k \tilde{H}(x_k)}, 0 \le O \le 1$$
(8)

The curve is further smoothed with a cubic B-spline. This treatment eliminates the jaggedness introduced by the discrete grid and renders the overlap rate distribution smoother for visualization and numerical integration. We define the normalized overlap area ratio (*NAR*) to convert the spatial curve into a single quantitative metric.

$$R = \frac{A_{overlap}}{A_{rect}} = \frac{1}{x_{max} - x_{min}} \int_{x_{min}}^{x_{max}} O(x) dx$$
 (9)

The numerator is the overlap rate distribution area $A_{overlap}$, evaluated by the trapezoidal rule on the discretized data; the denominator is the reference-rectangle area, A_{rect} , defined for the same width and unit height. Because O(x) is restricted to the range 0-1, the resulting ratio R likewise lies within [0, 1]. Physically, R represents the mean overlap rate along the radial direction. When R approaches 1, the diamond abrasives sweep the entire radial span uniformly, yielding more consistent wear and surface quality; by contrast, as $R \to 0$, the trajectories are highly concentrated in a localized region, which can lead to the severe local over-polishing of the pad.

3. Materials and Methods

3.1 Diamond conditioning disk design

In this study, we design and simulate a fixed diamond conditioning disk with microstructured single-crystal CVD diamond segments. Single-crystal diamond tiles of 10×10 and 0.5 mm thickness are employed, and dresser configurations containing three to twelve equally spaced diamonds (Fig. 1) are investigated. A corresponding tool-path simulation model is established to meet the dual requirements of polishing pad dressing uniformity and overall cost efficiency demanded by advanced CMP processes.

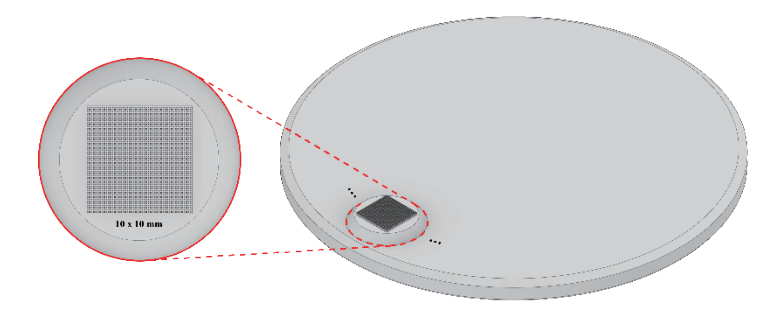


Fig. 1. (Color online) Design schematic of a micro-structured fixed diamond conditioning disk with single-crystal CVD diamond.

3.2 Simulation conditions

A numerical model of a representative planar CMP conditioning mechanism (Fig. 2) is constructed. The parameters listed in Table 1 were selected to represent a typical full-scale industrial CMP system, ensuring the practical relevance of the simulation findings. All geometric and kinematic parameters are set to this production scale. The polishing pad is a 510-mm-diameter disk whose centroid coincides with the global origin and rotates counterclockwise at a constant speed of 90 rpm. The diamond conditioning disk is mounted on the tip of the dresser arm. Driven by a servo actuator, the arm executes a three-stage motion: (i) from 0 to 2 s, it rotates from the home position to a preset angle; (ii) it remains stationary for the next 2 s; and (iii) it enters a $\pm 34^{\circ}$ oscillatory zone, reciprocating with a saw-tooth profile at 10° s⁻¹, as indicated by the arrowed sweep arc in Fig. 2. The diamond conditioning disk itself spins counterclockwise at a speed of 87 rpm. The combined pad rotation, arm oscillation, and disk spin form a multi-axis motion that faithfully reproduces the actual contact behavior of the diamonds against the pad during dressing.

4. Results and Discussion

4.1 Trajectory characteristics and overlap rate distribution

During dresser conditioning, the single-crystal diamond is driven by two coupled motions: the disk's self-rotation at the angular velocity ω_d and a harmonic lateral oscillation of the dressing arm along the x-axis, $x(t)=A\sin(2\pi f_{osc}t)$. Superimposing these components in polar coordinates (r,θ) produces an approximate Archimedean spiral $r=k\theta$ traced by the diamond's projected point on the pad surface (Fig. 3). The spiral feed rate k is jointly determined by the angular velocity difference $\Delta\omega=\omega_p-\omega_d$ and the oscillation amplitude A. Within a single revolution, this spiral path uniformly spans multiple radial pitches, thereby increasing cutting coverage and reducing local wear gradients.

For a 60 s path simulation, Fig. 4 illustrates how the global scanning trajectory on a 510-mm-diameter polishing pad evolves as the diamond count on the conditioning disk increases from N_d = 3 to 12.

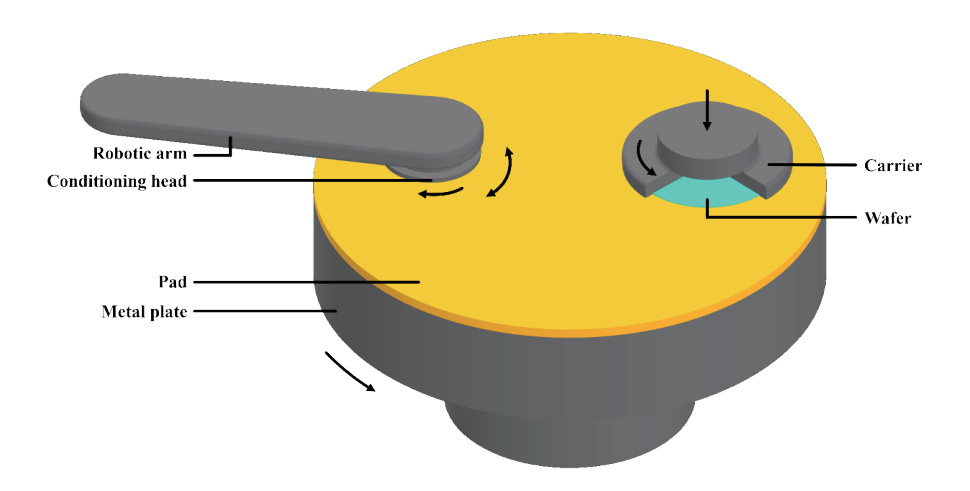


Fig. 2. (Color online) Geometric and kinematic schematic of the CMP polishing pad conditioning mechanism.

Table 1 CMP geometry and kinematic parameters.

_	1			
Category	Parameter	Symbol	Value	Unit
Geometry	Polishing pad diameter	D_{pad}	510	mm
	Diamond disk diameter	D_{DD}	101.6	mm
	Radius of diamond	r_{array}	40	mm
	Number of diamonds	N_d	3~12	_
Kinematics	Pad rotational speed	ω_{pad}	90	rpm
	Disk rotational speed	ω_{DD}	87	rpm
	Arm oscillation amplitude	A_{osc}	± 34	0
	Oscillation sweep rate	$\dot{ heta}_{osc}$	10	°/s

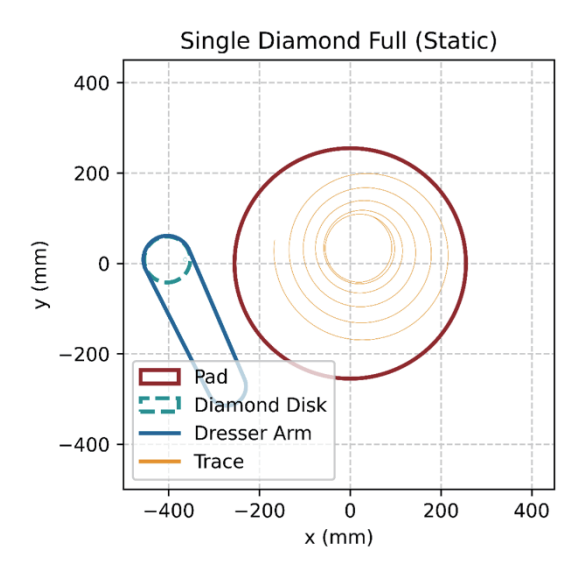


Fig. 3. (Color online) Path of a single diamond on the conditioning disk across the polishing pad.

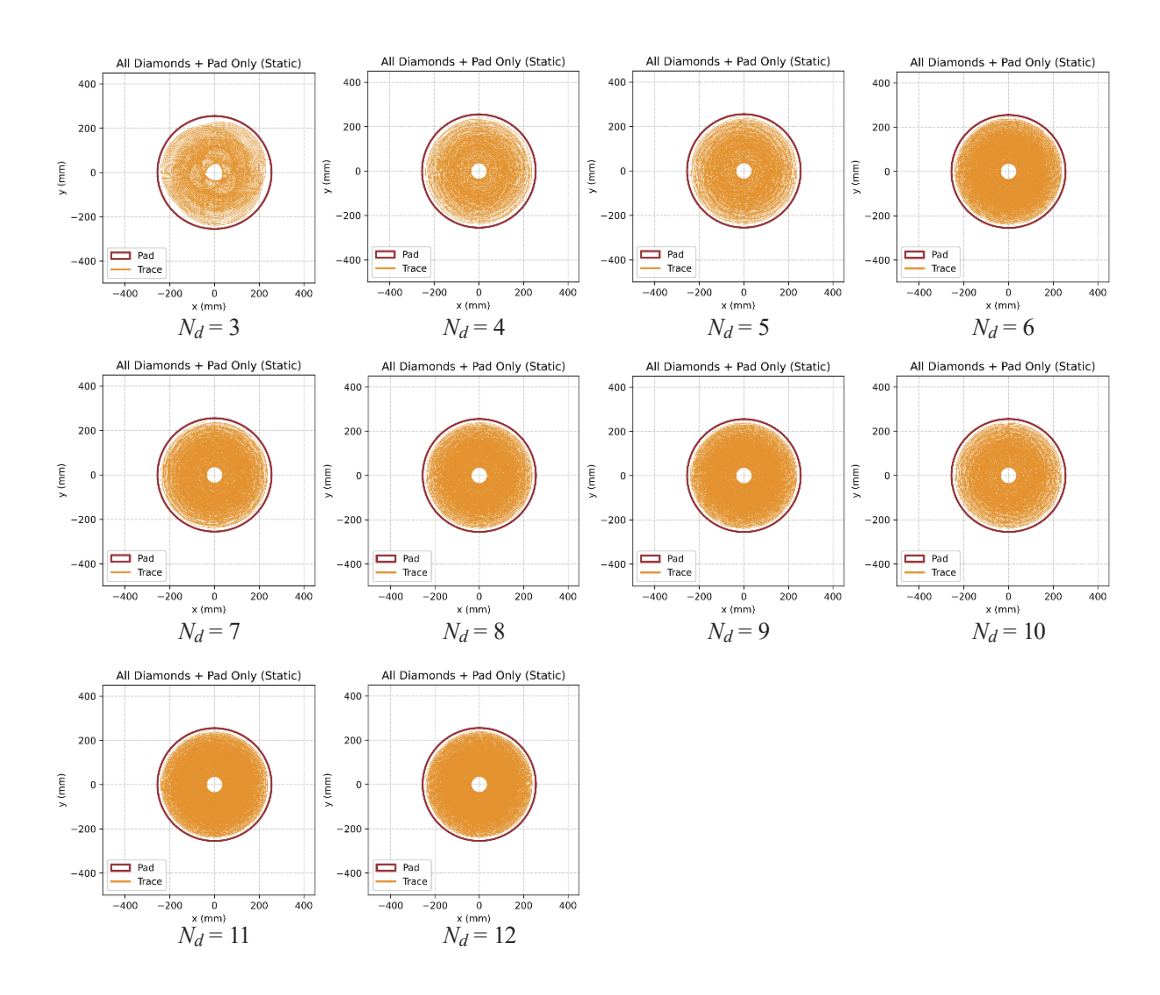


Fig. 4. (Color online) Global scanning trajectory of a multidiamond conditioning disk across the polishing pad.

- $N_d=3$. The three diamonds are equally spaced around the disk, resulting in an angular separation of $360^\circ/3=120^\circ$ between them. Consequently, each diamond traces its own Archimedean-like spiral path, but each path is phase-shifted by 120° relative to the others. This superposition of three distinct, phase-shifted trajectories produces the characteristic three-petal pattern of high hit density on the pad.
- $N_d = 4-6$. As the phase offset shrinks ($\Delta_{\varphi} = 360^{\circ}/N_d$), adjacent spiral "steps" begin to complement one another; blank regions narrow, but recognizable soft-rib bands persist.
- $N_d = 7-8$. Neighboring spirals almost fill one another's radial pitch. Hit-density contours become nearly concentric, and the central low-coverage zone contracts to about 40 mm, indicating optimal uniformity in both radial and angular directions.
- $N_d = 9$ –12. Additional diamonds mostly rescan regions with high density, making the trajectory visually denser yet yielding only marginal gains in adequate coverage. The central dead zone improves only slightly, whereas excessive overlap at the outer rim introduces a risk of over-cutting.

Figure 5 shows log-scale hit-density maps from a 60 s static simulation. As the number of diamonds on the conditioning disk rises from $N_d = 3$ to 12, the scanning pattern on the 510 mm polishing pad becomes notably denser: the peak hit density increases from 10^1 to roughly

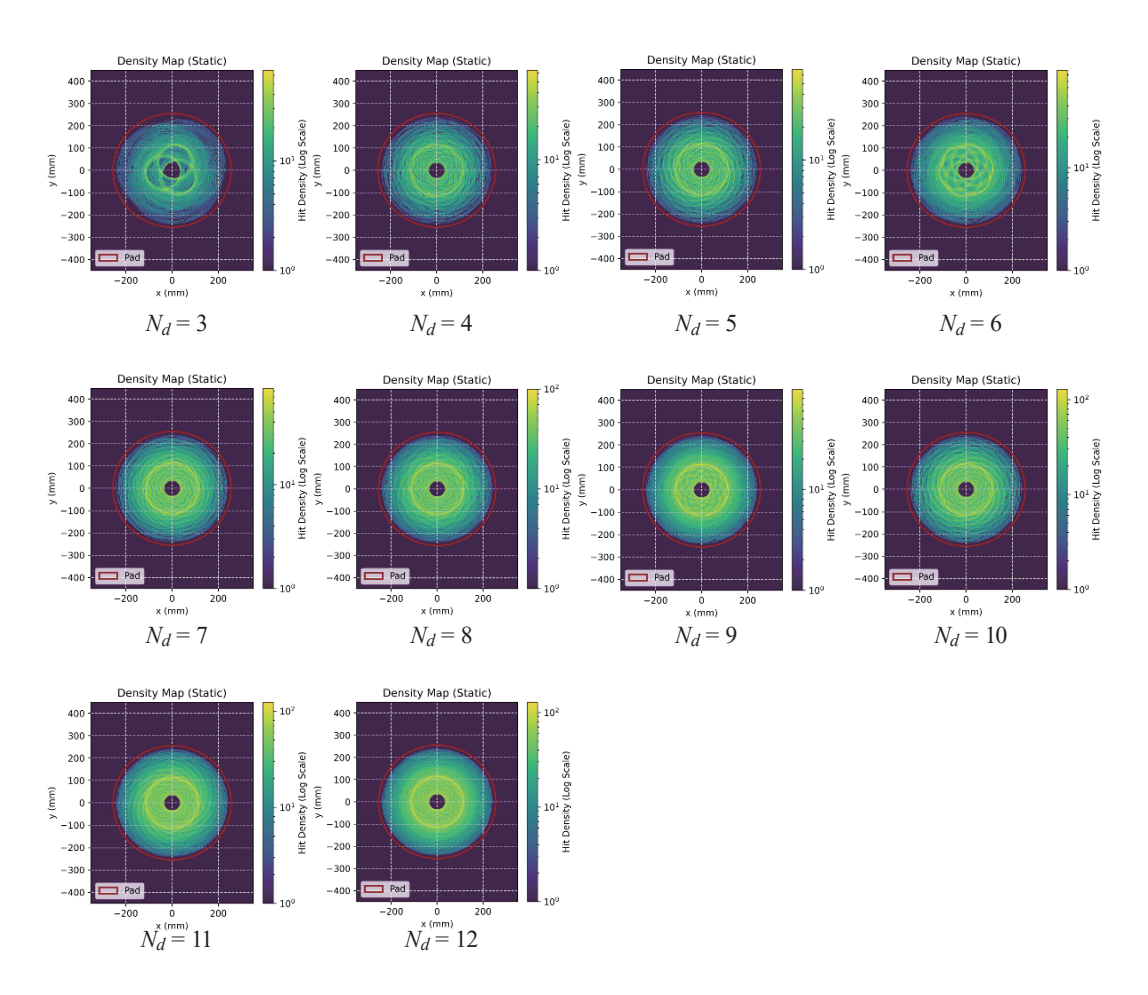


Fig. 5. (Color online) Density maps across the polishing pad generated by multidiamond conditioning disks.

10² hits/mm², and continuous ring-like contours gradually replace the original three-petal radial ridges. Once the diamond count exceeds eight, however, the additional diamonds mainly rescan zones that already have high density, so the gain in adequate coverage begins to saturate: the central low-hit valley closes only marginally, and the outer rim shows signs of local over-cutting owing to repeated passes. In other words, although the total number of trajectories grows with the diamond count, overlap efficiency exhibits diminishing returns. Eventually, it reaches a "high-density yet low-gain" plateau at the 10² hits/mm² level.

4.2 Impact of normalized area ratio and cost

The raw overlap ratio measured along the pad centerline (y = 0) was first peak-normalized to isolate the purely geometric effect of the diamond count on radial-coverage morphology. This step removes the total-area change associated with the absolute number of diamond and allows a focused comparison of relative variations in peak location, central-valley width, and flank-decay slope (Fig. 6). The normalized curves reveal that when the diamond count N_d increases from 3 to 6, the double-peak valley gradually narrows. Yet, a saw-tooth subharmonic envelope remains,

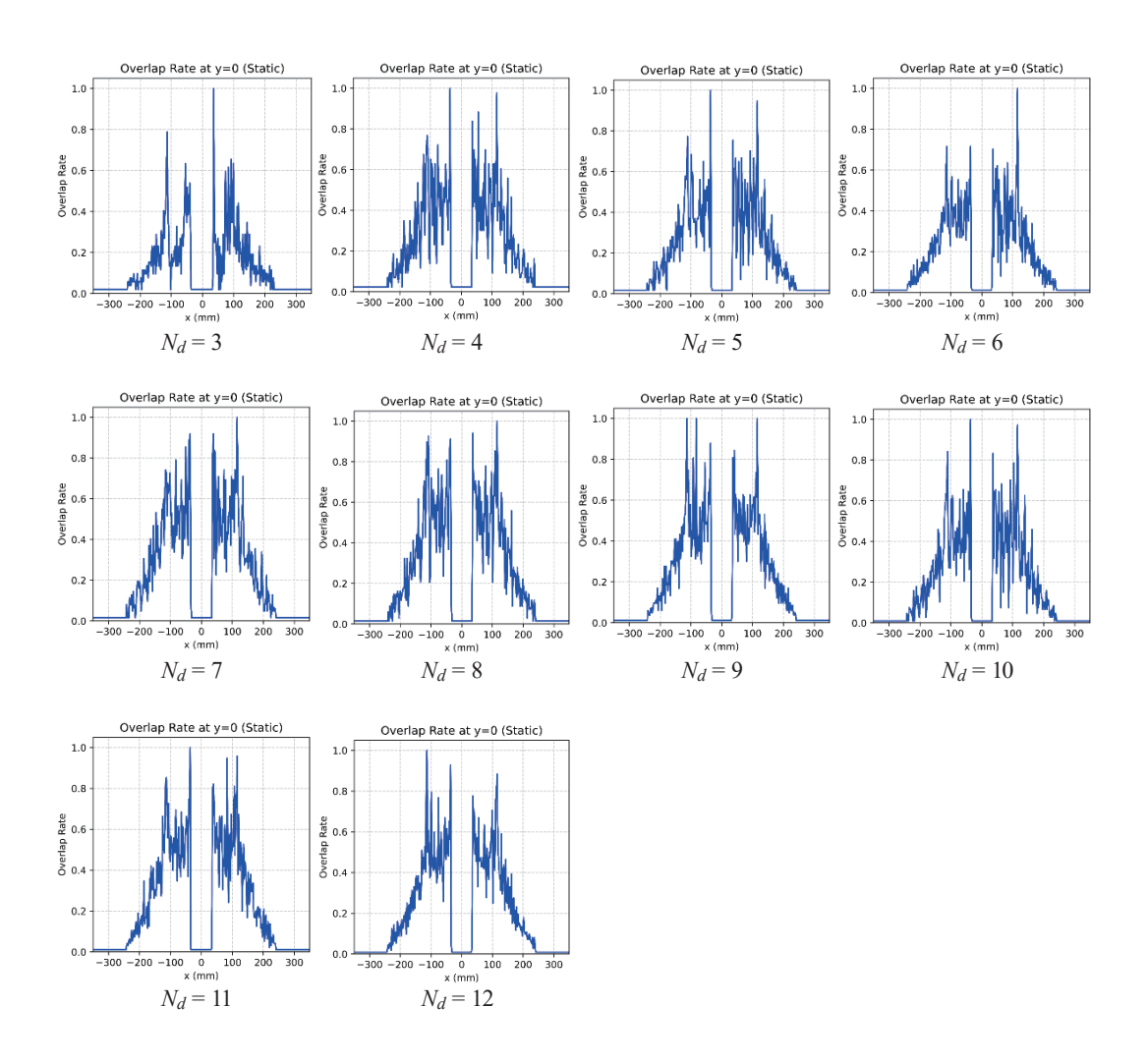


Fig. 6. (Color online) Normalized overlap rate profiles along the pad centerline (y = 0) for multidiamond conditioning disks.

indicating incomplete trajectory complementarity. At $N_d=7$ and 8, adjacent spiral pitches almost completely merge; the shoulders on both sides exhibit near-exponential smoothing, and radial and angular coverages reach their most uniform state. Further raising the count to $N_d=9$ –12 produces no appreciable change in peak amplitude (fixed by normalization); the central valley improves only marginally, while the curve shows more frequent sharp spikes, implying that additional diamonds mainly rescan already high-density regions, and the overlap efficiency therefore enters a regime of diminishing returns.

NAR does not rise monotonically with diamond count; instead, it fluctuates markedly (Fig. 7). Increasing the diamond count from three to four diamonds causes NAR to jump by +9.2%, whereas diamond counts of five and six lower the value. The global maxima appear at diamond counts of seven and eight (30.04 and 31.22%, respectively), indicating that this range offers the best geometric compensation. Although the cost continues to climb from diamond counts of nine to twelve, NAR saturates or declines because the additional diamonds mostly rescan regions already densely covered, pushing overlap efficiency into a regime of diminishing returns. The

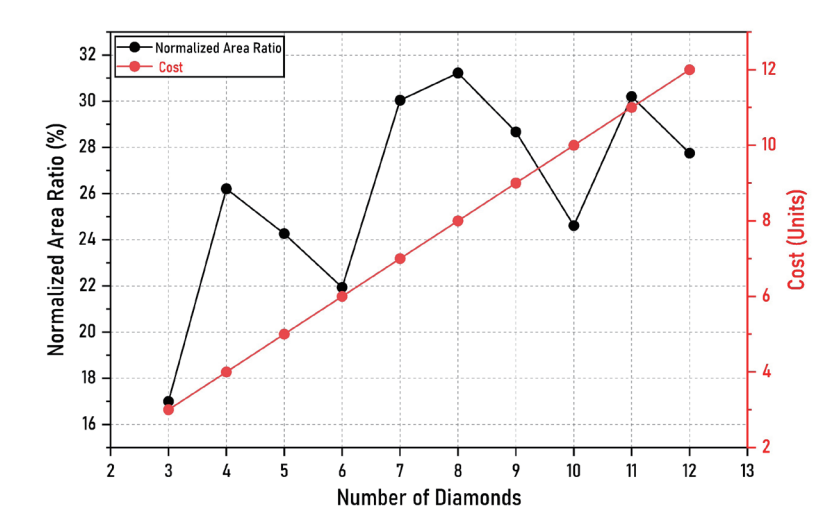


Fig. 7. (Color online) Combined effect of diamond count on *NAR* (left axis) and relative diamond conditioning disk cost (right axis). The cost is a relative unit directly proportional to the number of diamond segments.

diverging trends clarify that, when both performance and economics are considered, a configuration of seven to eight diamonds provides the optimal trade-off between normalized coverage and cost effectiveness.

5. Conclusions

Using a GPU-accelerated geometric-overlap model, we comprehensively quantified the scanning trajectories, overlap distribution, and cost-performance trade-offs of multidiamond conditioning disks during CMP. The results showed that, with a judicious diamond count and appropriate arm-sweep control, one can achieve highly uniform pad wear while maintaining economic viability.

(1) Spiral-plus-overlay path

A single diamond, driven by disk self-rotation and a $\pm 34^{\circ}$ oscillating arm, traces a near-Archimedean spiral that spans multiple radial pitches per revolution, effectively reducing local wear gradients.

(2) Optimal diamond count: seven to eight

The *NAR* exceeds 30% at seven to eight diamonds, eliminating the central low-impact region while keeping the diamond conditioning disk cost attractive.

(3) Drawbacks of excess diamonds

Beyond eight diamonds, the pad rim becomes over-conditioned; excessive overlap shortens pad life and increases slurry consumption, pushing the system into a regime of diminishing returns.

(4) Recommended multizone sweep speeds

A constant sweep rate over-conditions the pad center. Adopting a three-zone strategy, accelerating in the inner region and decelerating at the outer radius, stretches the trajectories, balances impact distribution, further improves uniformity, and extends pad lifetime.

(5) Rapid optimization guide and model scope

The framework serves as a rapid optimization guide, combining geometric visualization, the *NAR* metric, and cost analysis to predict how diamond layouts and arm parameters affect wear uniformity at the design stage. While this study was focused on the geometric coverage to provide a rapid and efficient optimization tool, it is essential to note that the model does not currently incorporate other complex physical phenomena such as slurry dynamics, pad deformation, or thermal effects. Integrating these multi-physics aspects represents a promising direction for future research to build a more comprehensive model. At the same time, the current framework can already be extended to other fixed-abrasive conditioners and materials to boost efficiency in advanced semiconductor CMP lines.

References

- 1 K. Schuegraf, M. C. Abraham, A. Brand, M. Naik, and R. Thakur: IEEE J. Electron. Devices Soc. 1 (2013) 66.
- 2 H. H. Radamson, A. C. Lindgren, L. Hultman, M. Kolahdouz, C. L. Hinkle, G. C. Tettamanzi, D. D. Nguyen, M. Ostling, and A. Lars, and M. O. Granstrom: Micromachines 10 (2019) 293.
- 3 M. Krishnan and M. F. Lofaro: Advances in Chemical Mechanical Planarization (CMP), S. Babu, Ed. (Woodhead Publishing, Cambridge, 2022) 2nd ed., pp. 29–50.
- 4 M. Morsy, F. Znid, and A. Farraj: Mater. Sci. Semicond. Process. 190 (2025) 109376.
- 5 M. Keswani and Z. Han: Developments in Surface Contamination and Cleaning, R. Kohli and K. L. Mittal, Eds. (William Andrew Publishing, Oxford, 2015) pp. 145–183.
- 6 M. Krishnan and M. F. Lofaro: Advances in Chemical Mechanical Planarization (CMP), S. Babu, Ed. (Woodhead Publishing, Cambridge, 2016) pp. 27–46.
- 7 Q.-P. Pham and C.-C. A. Chen: Int. J. Precis. Eng. Manuf. 18 (2017) 1683.
- 8 J. Seo: J. Mater. Res. 36 (2021) 235.
- 9 J. P. Wiff, Y. Tai, and K. Miyoshi: Fabrication of Chemical Mechanical Polishing (CMP) Pad Dresser by Using Chemical Reaction Between Diamond Abrasive Grains and Titanium Matrix, Materials Research Society Symp. Proc. (2010).
- 10 R. K. Singh and A. J. Galpin: Consumables for chemical mechanical planarization (CMP) (U.S. Patent 8444463, 2013).
- 11 M.-Y. Tsai, S.-T. Chen, Y.-S. Liao, and J. Sung: Int. J. Mach. Tools Manuf. 49 (2009) 722.
- 12 H. Cho, T. Lee, D. Kim, and H. Kim: Appl. Sci. 11 (2021) 4358.
- 13 N. Liu, P. Wu, F. Niu, T. Hou, and Y. Zhu: Precis. Eng. 81 (2023) 153.
- 14 N. Liu, P. Wu, J. Jia, and Y. Zhu: Mater. Manuf. Process. **39** (2024) 1933.
- 15 Q. Pham, N. V. Luc, and C.-C. Chen: Simulation of Cutting Locus and Overlap Cutting by Diamond Dressing in CMP Process (Preprint, 2019).

About the Authors



Yu-Chen Wang received his B.S. (2022) and M.S. (2024) degrees from National Chin-Yi University of Technology, Taiwan. His research interests include stress analysis, wafer inspection, processing, and materials characterization. (jack.xi1201@gmail.com)



Hong-Hui Lian received his B.S. (2020) and M.S. (2022) degrees from National Chin-Yi University of Technology, Taiwan. His research interests include silicon carbide chemical mechanical polishing (SiC-CMP), grinding, materials characterization, 3-D modeling, and photocatalysis. (lion941507@gmail.com)



Yue-Feng Lin received his B.S. degree from National Cheng-Kung University, Taiwan, in 2008 and his M.S. and Ph.D. degrees from National Cheng-Kung University, Taiwan, in 2009 and 2016, respectively. From 2017 to 2018, he was a postdoctoral researcher at the National Chin-Yi University of Technology, Taiwan. His research interests are in the machining and finishing of difficult-to-cut materials. (yflin@ncut.edu.tw)



Ming-Yi Tsai received her B.S. degree from the National Taiwan University of Science and Technology, Taiwan, in 1993 and her M.S. and Ph.D. degrees from National Taiwan University in 2000 and 2006, respectively. From 2007 to 2011, she was an assistant professor at the National Chin-Yi University of Technology, Taiwan. Since 2011, she has been a professor at the National Chin-Yi University of Technology, Taiwan. Her research interests are in cutting, grinding, and polishing technology. (mytsai@ncut.edu.tw)